Mechatronics 58 (2019) 82–92

Contents lists available at ScienceDirect

Mechatronics

journal homepage: www.elsevier.com/locate/mechatronics

Robust micro-positionnig control of a 2DOF piezocantilever based on an extended-state LKF

J. Escareno [a,*], J. Abadie [b], E. Piat [b], M. Rakotondrabe [b]

[a] XLIM Research Institute, UMR CNRS 7252, ENSIL-ENSCI / Université de Limoges, 16 Rue Atlantis, Limoges 87280, France
[b] FEMTO-ST Institute, University Burgogne Franche-Comt, CNRS UMR6174, UFC, ENSMM, UTBM 24 rue Alain Savary, Besancon 25000, France

ARTICLE INFO

Keywords:
Piezoelectric cantilever
Extended-state linear kalman filter
Robust micro-positioning
Disturbance estimation and compensation
Parametric and dynamic uncertainties
Bounded-input controller

ABSTRACT

This paper presents a control scheme regarding to improve the performances of a piezoelectric actuator (PEA) for precise positioning tasks. The piezoelectric actuator exhibits strong nonlinear disturbances for 1- and 2-DOF motion, i.e. input-dependent hysteresis, creep and cross-couplings. These unwanted phenomena undeniably compromise the final precision of the targeted tasks (micromanipulation) and therefore it should be conveniently considered during the controller synthesis. In this regard, the dynamic equation is also split into a nominal model and a uncertain model including parametric uncertainties. We propose to use simultaneously a the discrete linear extended-state linear Kalman filter (ES-LKF), to estimate the aforementioned disturbances and the velocity, and Lyapunov-based controller to guarantee asymptotic stability while meeting the actuator limits. The proposed strategy permits to perform accurate positioning, for regulation and trajectory-tracking tasks, without a prior knowledge of parametric and unmodeled uncertainties. Real-time experiments were carried out with circular trajectories to demonstrate the efficiency of the proposed approach.

1. Introduction

These last years, the advance of microrobotics has increasingly enhanced different applications. Particularly, in micromanipulation applications, technologies based on piezoelectric actuators represent a wide spectrum ranging from walking actuators, multi-DOF positioning systems to manipulation (transport and pick-and-place) of micro-sized objects. The advantageous performances profile provided by piezoelectric actuators (PEAs), bandwidth and resolution, is however degraded by static and dynamic disturbances (hysteresis and creep). Such PEAs adverse behavior depends on both current and past inputs. Hysteresis arises either in static regime (constant inputs) or dynamic regime (fast-/slow- time varying inputs). Furthermore, multi-DOF micropositioning applications bring unwanted cross-couplings for both sequenced or simultaneous motions.

The control of PEAs has been addressed using feedforward and feedback control approaches, or a combination of both. Feedforward-based schemes rely on the accuracy of the PEA's model and thus its inverse is able to compensate hysteresis reaching desired displacements. In the feedforward control of PEAs, several approaches are available to model and then to compensate for the hysteresis: the Preisach [1–3], the Prandtl-Ishlinskii [4–7] and the Bouc-Wen approaches [8,9]. In the two formers, a complex hysteresis is modeled by the sum of many basic hysteresis (hysterons). Both approaches can be very accurate with the use of a high number of elementary hysteresis, which represents a computational burden implementation. Alternatively, the Bouc-Wen model of hysteresis, has an interesting simplicity and is able to represent a large class of hysteresis. Although the low cost and the high packageability (no sensors required) of the used feedforward control approaches, their main limitation is the lack of robustness face to model uncertainties and to external disturbances.

On the other hand, feedback control has been used to deal with the motion control of PEAs. In this case, the controller's performances will be as good as the quality of the measurements and/or the estimation of the system's states, which in practice are noisy and/or missing (e.g. only position measurement is available). Two control applicative categories might be distinguished based on the control operational regime:

- *Regulation Task*
  In this regime, hysteresis, creep and couplings (multi-DOF PEAs) are considered as a constant disturbance introducing a static error. Thus, classical PID or event intelligent adaptive schemes can fullfil the control objective [10,11].
- *Trajectory-tracking Task*
  The aforementioned parasitic disturbances become dynamic. Therefore, robust control schemes are required to overcome significant

* Corresponding author.
E-mail addresses: juan.escareno-castro@unilim.fr (J. Escareno), jabadie@femto-st.fr (J. Abadie), epiat@ens2m.fr (E. Piat), mrakoton@femto-st.fr (M. Rakotondrabe).

https://doi.org/10.1016/j.mechatronics.2019.02.001
Received 21 April 2017; Received in revised form 24 December 2018; Accepted 3 February 2019

uncertainties. Recent works encompass sliding-mode control (SMC), SMC + adaptive and H_∞ schemes. Such controllers are able to reject the effect of the aforementioned disturbances [12–16].

State observers, either deterministic or stochastic, represent an interesting alternative for both operation profiles, not only to estimate missing states (e.g. velocity) and/or to improve state(s) measurement(s) (e.g. filtering [17]) but also to estimate unknown inputs (1DOF unknown input observers [18,19]) In this case, we have accomplished effective tracking of simultaneous time-varying trajectories (while rejecting inherent parasitic and dynamic uncertainties) having only position measurement while velocity is estimated from the ES-LKF. This reinforce and validates the proposed estimation and bounded-controller architectures. We are interested on (at micro/nano level) measurement resolution, displacement, and the accuracy of them and eventually their dynamics (see [20]). For this reason, it is important to have reliable sensory systems featuring such performance.

The present paper addresses a multi-DOF piezoelectric micro-positioning actuator devoted to dexterous micro-positioning tasks. The worst-case scenario corresponds to piezocantilever's simultaneous motion tracking a time-varying trajectory. Besides parasitic disturbances, input-dependent hysteresis and creep, input-interconnection couplings also degrades the positioning performance. From experimental observations on specific off-the-shelf piezocantilevers, we have witnessed that the parameters change during repeated test solicitation affecting the closed-loop effectiveness. Therefore, to apply the aforementioned control schemes for extensive trials requires a prior-to-trial identification phase. Alternatively we have proposed to split the dynamic model into a nominal model, that features initial identification parameters, and an uncertain parameters variations denoting the parametric disturbance. Both uncertainty terms, dynamic and parametric, are condensed into a overall lumped disturbance which will be further estimated. In order to overcome such evoked issues, we proposed and implemented in real-time a generalized disturbance compensation scheme based on an extended-state linear Kalman filter (ES-LKF) combined with a bounded-input controller. Unlike the previous works cited above, the actuator limits are considered within stability analysis which lies within the Backstepping technique. The asymptotically stability of the closed-loop system needs to be explicitly proven while experimental controllers are used due the nonlinear nature of the saturation of the actuator(s). Furthermore, for these kind of applications, if the voltage amplitude is too high, there is a risk of depolarization of the material leading to a loss of the piezoelectric properties. Consequently, overvoltages due to an excessive solicitation on the piezoelectric actuator to effectuate rapid responses (large bandwidth) or large courses may destroy the latter. Therefore, in this paper we design a controller that meets the real actuator's limits while providing asymptotic stability analysis. We have conducted an experimental stage to evaluate the trajectory tracking of the of the piezocantilever for a two-dimensional time-parametrized references trajectories, whose effectiveness is validated not only for the disturbance compensations (effective estimation) but also meeting the saturation limits of the controller. Furthermore, trajectory tracking of second order systems, as PEAs, requires the knowledge of both states.

The paper is organized as follows: the description and model of the piezocantilever is presented in section 2. In section 3 the characteristics of the experimental setup are described. In section 4 is described the LKF-based estimation algorithm as well as the closed-loop compensation scheme. Numerical and Experimental results are presented in Sections 5 and 6, respectively. Finally, the conclusions and perspectives are given in section 7.

2. Dynamic modeling of the piezocantilever

The actual paper considers as reference model for the piezocantilever the Bouc-Wen model of hysteresis, which corresponds to a cascade structure featuring a static hysteresis model plus a second order linear dynamic system (see Fig. 1). Such model stands out for its simplicity regarding computation and implementation. Another aspect is the compatibility of the Bouc-Wen model for controllers synthesis [8,9].

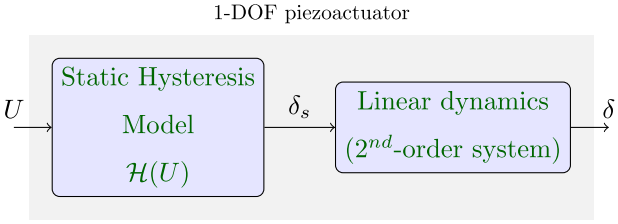

Fig. 1. Hammerstein Model of a 1-DOF Piezocantilever.

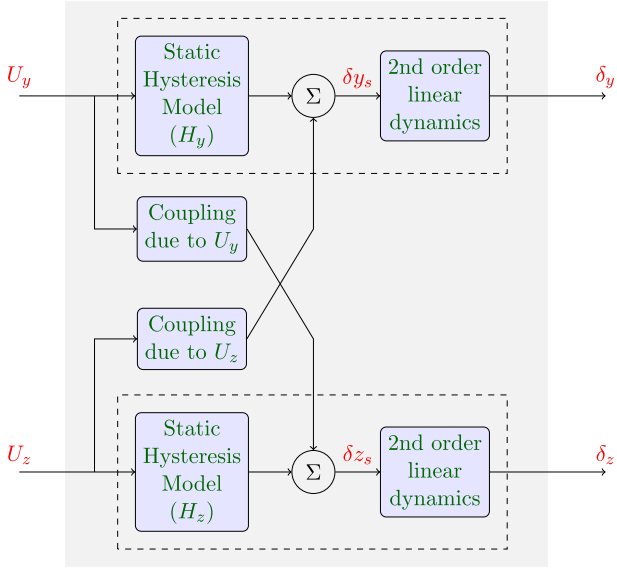

Fig. 2. Block scheme of coupling's structure.

The nonlinear equations which model the behavior of the multi-DOFs piezocantilever are written as

$$\begin{cases} a_i\ddot{\delta}_i + b_i\dot{\delta}_i + \delta_i = d_{pi}u_i - \mathcal{H}_i \\ \dot{\mathcal{H}}_i = d_{pi}A_{bwi}\dot{u}_i - B_{bwi}|\dot{u}_i|h_i - C_{bwi}\dot{u}_i|h_i| \end{cases} \tag{1}$$

where δ_i is the motion of the i−axis, $i \in \{y, z\}$ correspond to the bi-axial displacement, A_{bwi}, B_{bwi} and C_{bwi} are coefficients determining the hysteresis shape and amplitude and d_{pi} is a positive coefficient that defines the magnitude deflection, while h_i represents the hysteresis internal state. The dynamic parameters are denoted by a_i and b_i, which are obtained through an identification process. In our case, these parameters are set to a typical (or average) specifications of the piezocantilever.

2.1. Model extension

Single-axis positioning evolves in presence of hysteresis $\mathcal{H}_i$ and creep C_i, whereas, a bi-axial motion introduces a novel disturbances, generated by a dynamic input-interconnection couplings. The coupling effects are depicted (see Fig. 2). Such adverse couplings increase during simultaneous 2D operations, i.e. tracking a time-varying circular trajectories. From the latter we can regroup creep (for details see [4]) cross couplings into a generalized disturbance Θ_i, i.e.

$$\Theta_i = -\mathcal{H}_i + C_i + \mathcal{I}_i, \tag{2}$$

which allows to rewrite the nonlinear model (Eq. 1) as

$$a_i\ddot{\delta}_i + b_i\dot{\delta}_i + \delta_i = d_{pi}u_i + \Theta_i \tag{3}$$

where C_i the creep terms, $\mathcal{I}_i$ the interconnection disturbances (couplings). Moreover, in some cases the accuracy of the coefficients of the

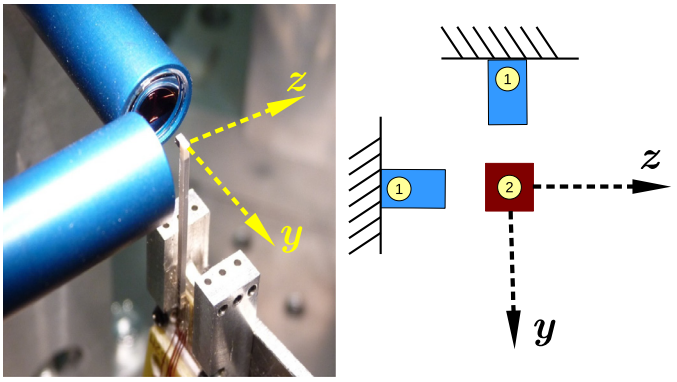

Fig. 3. Experimental setup is composed of two cofocal sensors arranged orthogonally (1) and a piezoelectric cantilever (2).

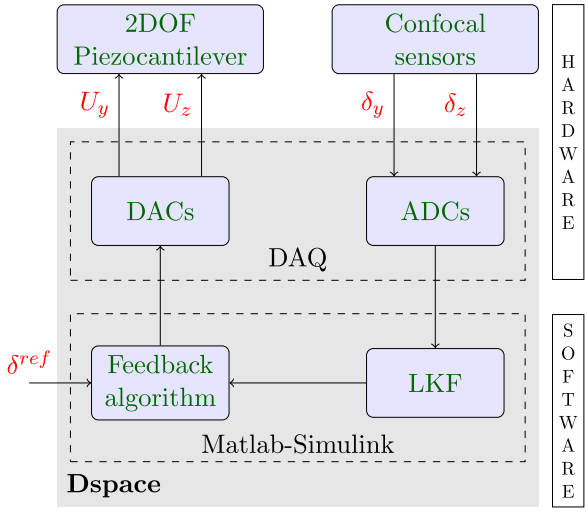

Fig. 4. Experimental architecture.

dynamic equation (Eq. 3) varies in function of the identification process quality. Then, (Eq. 3) is rewritten as

$$\underbrace{(a_{N_i}+\Delta_{a_i})}_{a_i}\ddot{\delta}_i+\underbrace{(b_{N_i}+\Delta_{b_i})}_{b_i}\dot{\delta}_i+\underbrace{(c_{N_i}+\Delta_{c_i})}_{c_i}\delta_i=d_{pi}u_i+\Theta_i, \tag{4}$$

where $(\cdot)_{N_i}$ stand for the nominal/characteristic/initial values of the model, $\Delta_{(\cdot)_i}$ the parametric uncertainties. From the latter structure it is possible to include such parametric uncertainties into a lumped disturbance Θ_i reducing the system (Eq. 4) to

$$a_{N_i}\ddot{\delta}_i+b_{N_i}\dot{\delta}_i+c_{N_i}\delta_i=d_{pi}u_i+\Theta_i \tag{5}$$

with

$$\Theta_i=\underbrace{-\mathcal{H}_i+C_i+\mathcal{I}_i}_{\text{parasitic nonlinearities}}-\underbrace{(\Delta_{a_i}\ddot{\delta}_i+\Delta_{b_i}\dot{\delta}_i+\Delta_{c_i}\delta_i)}_{\text{parametric uncertainties}} \tag{6}$$

3. Experimental setup description

The experimental positioning system features a 2DOF piezocantilever which evolves along the y and z axes. This actuator is designed with 36 piezo-electric layers to work at low input voltage. The total dimensions of the active part are 25x1x1 mm^3. This cantilever is controlled by two inputs U_y and U_z that are varying in the range of ± 20 volts. The first extremity of the cantilever is clamped while the other moves within the 2D $y-z$ plane based on the input U_i with $i\in\{y, z\}$ (see Figs. 3 and 4).

Table 1
Dynamic parameters of the piezocantilever.

Parameter (y-axis)	value	Parameter (z-axis)	value
a_{N_y}	4.4209×10^{-9}	a_{N_z}	3.5125×10^{-9}
b_{N_y}	$3.7378\times^{-6}$	b_{N_z}	2.9062×10^{-5}
d_{p_y}	5.13	d_{p_z}	3.702

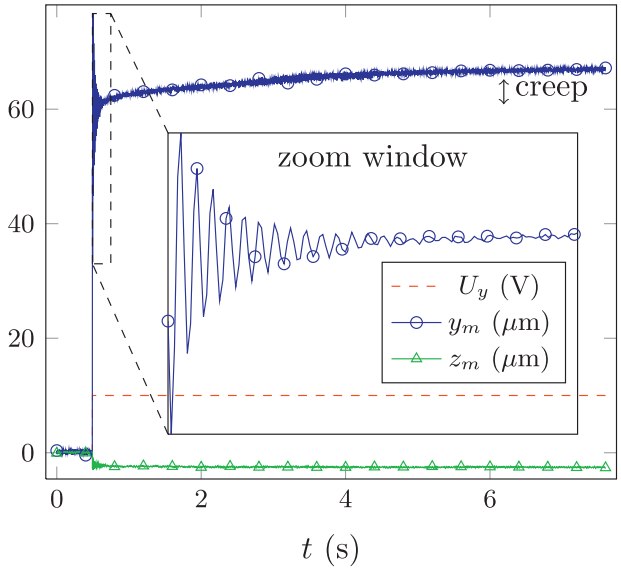

Fig. 5. Piezocantilever step response to a 10V step input U_y ($U_z=0$).

3.1. Model identification

The parameters corresponding to the coefficients of the dynamic equation (Eq. 1) of the piezocantilever have been identified using the ARMAX approach (Autoregressive-moving-average model with exogenous inputs) with an experimental 10 Volts step response applied to the piezocantilever (see Table 1). For the sake of comprehension Fig. 5 illustrate the signals used for the identification process for the $y-$axis and its effect on the $z-$axis.

The cantilever displacement in the 2D yz-plane is given by δ_i, with $i\in\{y, z\}$. The measurement of δ_i is acquired by two external confocal sensors orthogonally arranged aiming at the piezocantilever's tip (see Fig. 3).

4. Estimation and control strategy

A discrete linear Kalman filter (LKF) is designed and implemented in real-time to estimate the static and dynamic disturbances for a two-dimensional micro-positioning task of the piezocantilever. The Linear Kalman Filter (LKF) is derived from a 2nd-order continuous state-space system

$$\begin{cases}\dot{x}(t)=Ax(t)+Bu(t)+\mathcal{M}\omega(t)\rightarrow\text{process}\\ y(t)=Cx(t)+\nu(t)\rightarrow\text{sensor(s)}\end{cases} \tag{7}$$

where the state vector $x=(\delta_i,\dot{\delta}_i)^T$. This model considers the following hypothesis:

H1. The pair AC verifies the observability property
H2. The terms $\omega(t)=(\omega^{\delta_i},\omega^{\dot{\delta}_i})^T$ and $\nu(t)=(\nu^{\delta_i},\nu^{\dot{\delta}_i})^T$ stand for a white Gaussian random process respectively and represent the uncertainties in the process and outputs (sensors). Such terms verify

$$E[\omega(t)]=0 and\, E[\nu(t)]=0 \tag{8}$$

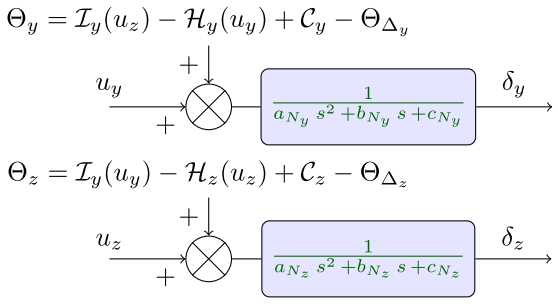

Fig. 6. Simplified disturbed model.

with constant power spectral density (PSD) $W(t)$ and $V(t)$ respectively.

The covariance matrix of the model

$$Q = E\left[\omega(t)\omega(t)^T\right] = \text{diag}\left[\sigma^2(\omega^{\delta_i}), \sigma^2(\omega^{\dot{\delta}_i})\right] \tag{9}$$

The sensor covariance matrix

$$R = E\left[\nu(t)\nu(t)^T\right] = \text{diag}\left[\sigma^2(\nu^{\delta_i}), \sigma^2(\nu^{\dot{\delta}_i})\right] \tag{10}$$

It is also assumed that both stochastic processes are not correlated, i.e.

$$E\left[\omega(t)\nu(t)^T\right] = 0 \tag{11}$$

4.1. Disturbance estimation based on ES-LKF

Let us recall the piezocantilever model given by Eq. (5)

$$a_{N_i}\ddot{\delta}_i + b_{N_i}\dot{\delta}_i + c_{N_i}\delta_i = d_{pi}u_i + \Theta_i \tag{12}$$

This model corresponds to two scalar disturbed systems defining the motion behavior along y and z axes (see Fig. 6). This model may be rewritten into the state-space representation

$$\begin{aligned} \dot{x} &= Ax + Bu + Pd \\ y &= Cx \end{aligned} \tag{13}$$

The positions δ_i are provided by the confocal chromatic sensors and $d = \Theta_i$ corresponds to the dual-axis disturbance. The velocity is obtained via the estimation provided by the LKF. The matrices of the system (Eq. 13) are given by:

$$A = \begin{pmatrix} 0 & 1 \\ -\frac{c_i}{a_i} & -\frac{b_i}{a_i} \end{pmatrix} B = \begin{pmatrix} 0 \\ \frac{d_{pi}}{a_i} \end{pmatrix} P = \begin{pmatrix} 0 \\ \frac{1}{a_i} \end{pmatrix} C = \begin{pmatrix} 1 & 0 \end{pmatrix} \tag{14}$$

It is assumed that no prior information about the disturbance is available. However, we consider that the disturbance has a slow time-varying dynamics that can be modeled by a random walk process

$$\dot{\Theta}_i = \omega^{\Theta_i}, \tag{15}$$

where $\omega^e(t) = (\omega^{\delta_i}, \omega^{\dot{\delta}_i}, \omega^{\Theta_i})^T$. The latter assumption allows us to introduce an extended state-space vector:

$$x^e = (\delta_i, \dot{\delta}_i, \Theta_i)^T \tag{16}$$

and its associated extended-state model describing the dynamics is obtained from (Eq. 15) in which the unknown input disturbance Θ_i is incorporated in the transition matrix:

$$\dot{x}^e = \mathcal{A}x^e + \mathcal{B}u + \mathcal{M}\omega^e \tag{17}$$

$$y = Cx^e + \nu \tag{18}$$

with

$$\mathcal{A} = \begin{pmatrix} 0 & 1 & 0 \\ -\frac{c_i}{a_i} & -\frac{b_i}{a_i} & \frac{1}{a_i} \\ 0 & 0 & 0 \end{pmatrix} \quad \mathcal{B} = \begin{pmatrix} 0 \\ \frac{d_{pi}}{a_i} \\ 0 \end{pmatrix} \tag{19}$$

$$\mathcal{M} = \begin{pmatrix} 1 & 0 & 0 \\ 0 & 1 & 0 \\ 0 & 0 & 1 \end{pmatrix} \quad C = \begin{pmatrix} 1 & 0 & 0 \end{pmatrix} \tag{20}$$

The continuous-time model (Eq. 17) can be discretized with sampling time T_s and considering a zero-order hold (zoh) yield

$$x^e_{k+1} = \mathcal{A}_k x^e_k + \mathcal{B}_k u_k + \omega_k \tag{21}$$

$$y_k = C_k x^e_k + \nu_k \tag{22}$$

with

$$x^e_k = \left(\delta_{i_k}, \dot{\delta}_{i_k}, \Theta_{i_k}\right)^T \tag{23}$$

$$\mathcal{A}_k = e^{\mathcal{A}T_s} \tag{24}$$

$$\mathcal{B}_k = \left(\int_0^{T_s} e^{\mathcal{A}T_s}\right)\mathcal{B} \tag{25}$$

$$\omega^e_k = \left(\omega^{\delta_i}_k, \omega^{\dot{\delta}_i}_k, \omega^{\Theta_i}_k\right)^T \tag{26}$$

$$\nu^e_k = \nu^{\delta_i}_k \tag{27}$$

where ω_k and ν_k are discrete-time band-limited white gaussian random process with zero-mean characterizing uncertainties on the model (unmodeled dynamics and parametric uncertainties) and measurement (noisy sensors) equations, respectively. The model uncertainties discrete covariance matrix Q_k is:

$$Q_k = E\left[\omega^e_k \omega^{e^T}_k\right] = \int_0^{T_s} e^{\mathcal{A}t}\mathcal{M}Q\mathcal{M}^T e^{\mathcal{A}^T t} dt \tag{28}$$

where the continuous covariance matrix stands for

$$Q = \text{diag}\left[\sigma^2\left(\omega^{\delta_i}_k\right), \sigma^2\left(\omega^{\dot{\delta}_i}_k\right), \sigma^2\left(\omega^{\Theta_i}_k\right)\right] \tag{29}$$

The algorithm that computes the estimate (including the disturbance Θ_i) of the state vector x^e_k is initialized as follows:

- The piezocantilever-based micro-positioning system is in the equilibrium state

$$x^e_{k_0} = (0, 0, 0)^T \tag{30}$$

- The initial covariance matrix P_0 is considered as

$$P_0 = \text{diag}\left[\sigma^2(\delta_{i_0}), \sigma^2(\dot{\delta}_{i_0}), \sigma^2(\Theta_{i_0})\right] \tag{31}$$

The corresponding LKF recursive algorithm features a prediction-estimation structure and is provided next

$$\begin{aligned} &\texttt{Prediction stage} \\ \hat{x}_{est_k} &= \mathcal{A}_k \hat{x}_{est_k} + \mathcal{B}_k u_k \\ P_{pred_k} &= \mathcal{A}_k P_{est_k} \mathcal{A}^T_k + Q \\ K_k &= P_{pred_k} C^T_k \left(C_k P_{pred_k} C^T_k + R\right)^{-1} \\ &\texttt{Estimation stage} \\ y_k &= \text{measurement vector} \\ \hat{x}_{est_k} &= \hat{x}_{pred_k} + K_k\left(y_k - C_k \hat{x}_{pred_k}\right) \\ P_{est_k} &= \left(I - K_k C_k\right) P_{pred_k} \left(I - K_k C_k\right)^T \end{aligned}$$

where K_k denotes the Kalman filter gain, and I is the identity matrix. The estimated vector state generated by the LKF is the written:

$$\hat{x}^e_k = (\hat{\delta}_{i_k}, \hat{\dot{\delta}}_{i_k}, \hat{\Theta}_{i_k})^T \tag{32}$$

For the actual work it was considered

$$\hat{\Theta}_{i_k} = C_d \hat{x}^e_k \tag{33}$$

with $C_d = (0, 0, 1)^T$

4.2. Bounded-input controller design

Assuming the knowledge of the disturbance $\hat{\Theta}_{i_k}$, the goal consists in driving the equilibrium point of the actual piezoactuator through a controller whose asymptotic stability is demonstrated, but also a controller that meets the actuator's limits (saturation). To this end, the Backstepping technique provides an appropriate framework to construct the controller since the aforementioned dynamic model (Eq. 12) features a cascade form suitable to apply such control technique.

Let us remind the dynamic model by assuming that the voltage $u(t)$ is within the limitation:

$$\ddot{\delta} = \frac{d_p}{a}u - \frac{b}{a}\dot{\delta} - \frac{1}{a}\delta + \Theta \tag{34}$$

Where we have dropped the subscript i and $N$to avoid notation abuse. Since we are concerned on solving the trajectory tracking problem, the latter dynamic model is rewritten in terms of the error ξ. To do so, the control input must contain the reference dynamic $\ddot{\delta}^d$. Thus, the control input is written

$$u = \frac{a}{d_p}\left[u^\star + \ddot{\delta}^d + \tanh\left(\frac{b}{a}\dot{\hat{\delta}} + \frac{1}{a}\delta\right)\right] \tag{35}$$

where $u^\star$ will be designed later. Introducing (Eq. 35) in (Eq. 34) leads to cancel out the nominal dynamics, after an arbitrary time t_1, since the piezocantilever features a stable behavior, i.e.

$$\lim_{t\to t_1}\tanh\left(\frac{b}{a}\dot{\hat{\delta}} + \frac{1}{a}\delta\right) = \frac{b}{a}\dot{\hat{\delta}} + \frac{1}{a}\delta \tag{36}$$

Through (Eq. 35) it is possible to perform a coordinates change allowing to rewrite the system in terms of the error.

$$\ddot{\xi} = \ddot{\delta} - \ddot{\delta}^d = u^* + \Theta \tag{37}$$

whose state-space representation is

$$\begin{aligned}\dot{\xi}_1 &= \xi_2\\ \dot{\xi}_2 &= u^\star + \Theta\end{aligned} \tag{38}$$

where $\xi_1 = \delta - \delta(t)^d$ and $\xi_2 = \dot{\hat{\delta}} - \dot{\delta}^d(t)$ are the position and velocity errors, respectively.

Remark. For trajectory tracking purposes, i.e. stabilizing the system (Eq. 38), requires the full knowledge of the vector state $x = (\delta, \dot{\delta})^T$ and only position is measured. Thus, the state-vector is completed with the LKF-based velocity estimation $\dot{\hat{\delta}}$.

4.2.1. Stability analysis

Before proceeding with the control design, let us present the following useful properties

- **P1.** $\tanh(\chi) \le \chi$
- **P2.** $1 \ge \sec^2(\chi) > 0$
- **P3.** $-\chi < -\tanh(\chi)$
- **P4.** $-\chi^2 < -\tanh^2(\chi)$

where $\chi \in \mathbb{R}^n$. In order to synthesize the controller we use the Backstepping technique. Backstepping starts (stabilizes) with the first integrator (position) by introducing a virtual controller and continue in this sense until reaching the control input at the last step (for details see [21]).

Step 1: Let us propose the Candidate Lyapunov Function (CLF) to deduce a control that provide global asymptotic stability (GAS) for the first integrator subsystem (Eq. 38a)

$$\mathcal{V}_1 = \frac{1}{2}\tanh^2(\xi_1) \tag{39}$$

whose the time-derivative

$$\dot{\mathcal{V}}_1 = \tanh(\xi_1)\mathrm{sech}^2(\xi_1)\xi_2 \tag{40}$$

using **P2** (Eq. 39) is rewritten as

$$\dot{\mathcal{V}}_1(\xi) \le \tanh(\xi_1)\xi_2 \tag{41}$$

which is rendered negative-definite ($\dot{\mathcal{V}}_1(\xi) < 0$) provided that

$$\xi_2 = -\lambda_1\tanh(\xi_1) \tag{42}$$

where λ_1 is a positive scalar gain. Hence, we can conclude that ξ_1 is not only stable but also converges asymptotically to the origin.

Step 2: Let us define an error state variable z for ξ_2, where the previous virtual controller is used as a reference in order to impose a constrained behavior, i.e. $\xi_2^d = -\lambda_1\tanh(\xi_1)$. Thus, let us consider

$$\tanh(z) \triangleq \xi_2 - \xi_2^d = \xi_2 + \lambda_1\tanh(\xi_1) \tag{43}$$

from which the state is given

$$\xi_2 = \tanh(z) - \lambda_1\tanh(\xi_1) \tag{44}$$

Differentiating (Eq. 43) yield

$$\mathrm{sech}^2(z)\dot{z} = \dot{\xi}_2 + \mathrm{sech}^2(\xi_1)\dot{\xi}_1 = \dot{\xi}_2 + \mathrm{sech}^2(\xi_1)\lambda_1\xi_2 \tag{45}$$

At this point, using (Eqs. 44) and (45), the model (Eq. 38)

$$\begin{aligned}\dot{\xi}_1 &= \tanh(z) - \lambda_1\tanh(\xi_1)\\ \dot{z} &= \frac{1}{\mathrm{sech}^2(z)}\left[u^\star + \Theta + \lambda_1\mathrm{sech}^2(z)(\tanh(z) - \lambda_1\tanh(\xi_1))\right]\end{aligned} \tag{46}$$

Let the final CLF be

$$\mathcal{V}_2 = \frac{1}{2}\tanh(\xi_1)^2 + \frac{1}{2}\tanh^2(z) \tag{47}$$

Obtaining the corresponding time-derivative of $\mathcal{V}_2(\xi_1, z)$ and using **P2** yields

$$\dot{\mathcal{V}}_2 \le \tanh(\xi_1)\xi_2 + \tanh(z)\dot{z} \tag{48}$$

Using (Eq. 46) in (Eq. 48) leads to

$$\begin{aligned}\dot{\mathcal{V}}_2 = &-\lambda_1\tanh^2(\xi_1) + \tanh(\xi_1)\tanh(z)\\ &+ \tanh(z)\left[u^\star + \Theta + \lambda_1\tanh(z) - \lambda_1^2\tanh(\xi_1)\right]\end{aligned} \tag{49}$$

In order to render (Eq. 49) into a negative-definite function, we introduce the following controller through the error dynamics $\ddot{\xi}$ (Eq. 38b).

$$u^\star = -\hat{\Theta} - \tanh(z)(\lambda_1 + \lambda_2), \tag{50}$$

where $\lambda_2 > 0$ is the second gain and also it is considered that δ and $\dot{\delta}$ are origin-convergent states, indicating that after some time τ_1 they lie into the linear domain of $\tanh(\cdot)$. Introducing the controller (Eq. 50) via $\dot{\xi}_2$ (see Eq. 38) in (Eq. 49) leads to

$$\dot{\mathcal{V}}_2 = -\tanh^2(\xi_1) + (1 - \lambda_1^2)\tanh(\xi_1)\tanh(z) - \lambda_2\tanh^2(z) \tag{51}$$

considering **P3** and **P4** (Eq. 51) is rewritten as

$$\dot{\mathcal{V}}_2 \le -\xi_1^2 + \left(1 - \lambda_1^2\right)\xi_1 z - \lambda_2 z^2 \tag{52}$$

As long as $\lambda_1 > 1$ and $\lambda_2 > 0$, $\dot{\mathcal{V}}_2 \le 0$ which guarantees stability of the origin and boundedness of the solutions as $t \to \infty$, i.e.

$$\|(\xi, z)^T\| \le \gamma, \tag{53}$$

where $\gamma \in \mathbb{R}^+$ stands for the stability region radius. However, we are interested in drawing conclusions about asymptotic stability of the states vector. For this reason, let us consider $\nu = (\xi, z)^T$ and

$$A = \begin{pmatrix} \lambda_1 & -\frac{1-\lambda_1^2}{2}\\ -\frac{1-\lambda_1^2}{2} & \lambda_2\end{pmatrix} \tag{54}$$

which allows to rewrite (Eq. 52) as

$$\dot{\mathcal{V}}_2 = -\nu^T A\nu \tag{55}$$

which is definite negative if A is positive definite, i.e. $\det[A] > 0$. The latter holds if

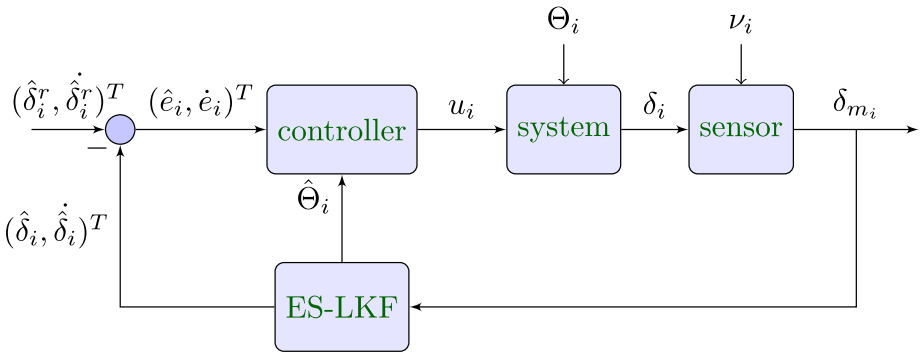

Fig. 7. Closed-loop architecture.

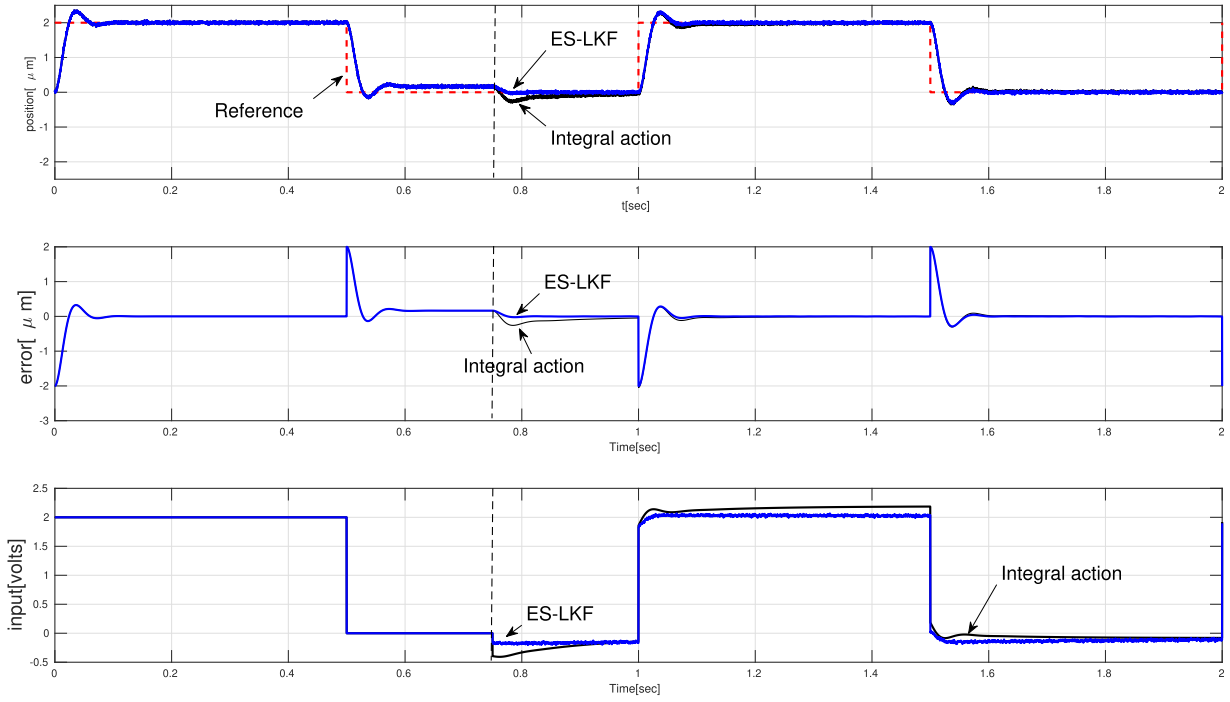

Fig. 8. case 1: performance comparison for switching constant reference.

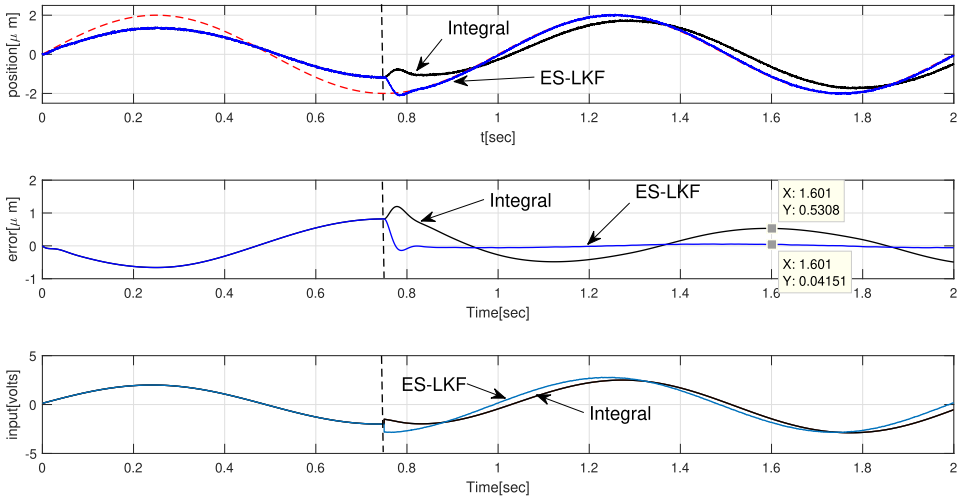

Fig. 9. case 2: performance comparison for time-varying sinusoidal reference.

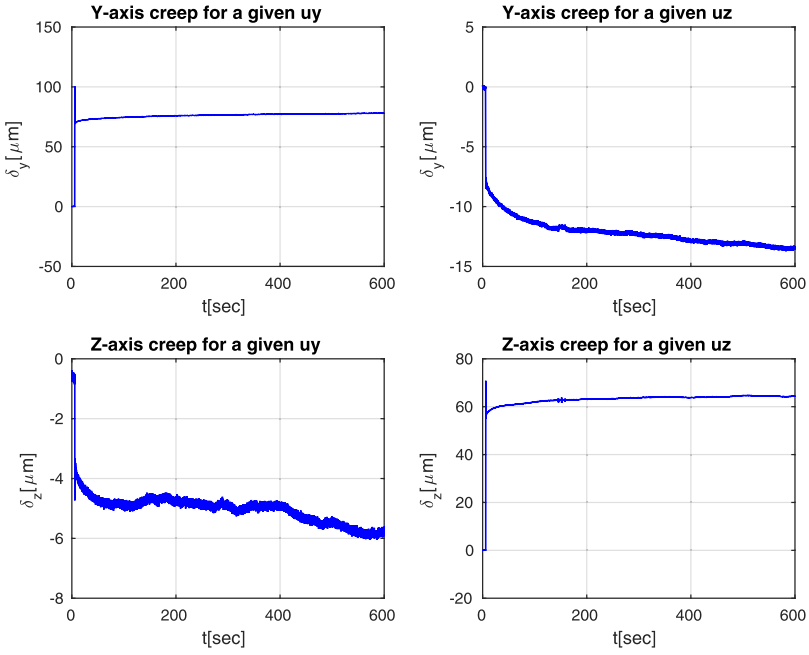

Fig. 10. Curves depicting the creep effect and its dual-axis coupling phenomena for an input of 10V in both axes.

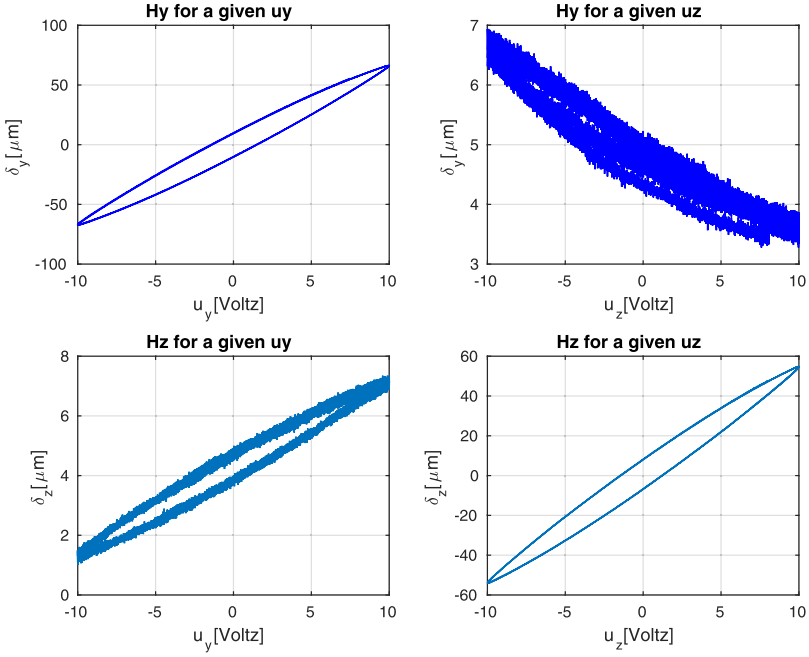

Fig. 11. Curves depicting the hysteresis effect and its dual-axis coupling phenomena for a 10V sinusoidal input.

- $\lambda_1^2 > 1$
- $\lambda_2 > \frac{(1-\lambda_1^2)^2}{4\lambda_1}$,

and whose negativity is assured, since the upper bound remains negative, i.e.

$$\dot{\mathcal{V}}_2 \leq -\alpha_{min}\{A\}\|\nu\|^2 \tag{56}$$

where $\alpha_{\min}\{\cdot\}$ stands for the minimum eigenvalue. Thus, $\dot{\mathcal{V}}_2 < 0$ and hence the state-vector trajectories converge asymptotically to the origin, i.e. $\xi_1 \to 0$ and $z \to 0$, this means that $\xi_2 \to \tanh(\xi_1)$ fulfilling the tracking objective.

Therefore, replacing (Eq. 50) in (Eq. 35) we obtain the final expression of the controller written as

$$u = \frac{a}{d_p}\left[-\hat{\Theta} - \tanh(z)(\lambda_1 + \lambda_2) + \ddot{\delta}^d + \tanh\left(\frac{b}{a}\dot{\hat{\delta}} + \frac{1}{a}\delta\right)\right]$$

5. Numerical results: A comparative study

In order to motivate the proposed strategy, we present, for comparative purposes, two control scenarios: the regulation and tracking problems in 1DOF. We observe the disturbance rejection performance of the PID versus the disturbance compensation based on the ES-LKF. For the actual simulation study we have considered only the hysteresis ($\mathcal{H}(t)$). The parameters used in the simulation are depicted in Table 2.

The control integral and ES-LKF-based are described next:

- Since the piezocantilever system (1) features a stable dynamic behavior (natural PD) we add an integral term, with gain $k_i = 10$, activated

$$u = \frac{a}{d_p}\left(\frac{1}{a}\delta^d + \frac{b}{a}\dot{\delta}^d + \ddot{\delta}^d - \frac{k_i}{a}\int_0^t \varepsilon(\tau)d\tau\right) \tag{57}$$

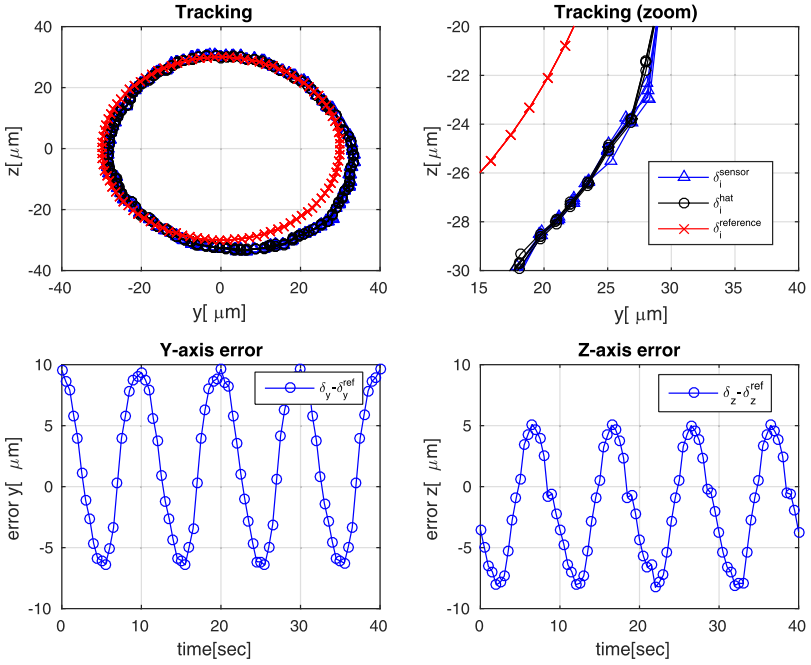

Fig. 12. Open-loop performance @ 0.1*Hz*.

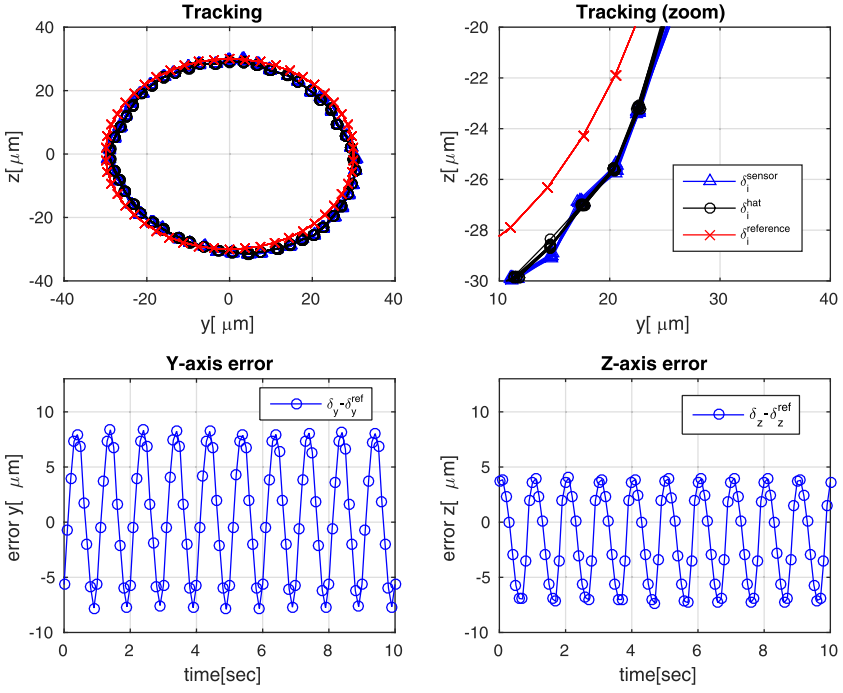

Fig. 13. Open-loop performance @ 1*Hz*.

Table 2
Dynamic parameters of the piezocantilever.

Parameter	Value
a_N	0.1×10^{-3}
b_N	$0.1\times^{-1}$
d_p	4.1083

where $\epsilon = \delta - \delta^d$.

- Next, we have replaced the integral term by the estimation of the disturbance via the ES-LKF.

$$u = \frac{a}{d_p}\left(\frac{1}{a}\delta^d + \frac{b}{a}\dot{\delta}^d + \ddot{\delta}^d + \hat{\mathcal{H}}(t)\right) \tag{58}$$

For both cases we activate the control action at $t = 0.75[s]$. Let us consider the following cases:

1) **Regulation case:** we consider a step sequence reference (frequency= $1[Hz]$ and amplitude= 2[μm]). Thus, the desired position δ^d is a constant reference toggling from $\delta^d = 0[\mu m]$ and $\delta^d = 2[\mu m]$.
Remark. In Fig. 8 it is depicted the numerical results where we have noticed that in steady-state the performance that both approaches eliminate the static error. However, within the transitory phase the overshoot smaller with ES-LKF approach. It is noteworthy that bigger values of for integral gain k_i ($k_i > 10$) increase the overshoot and provides a underdamped behavior.

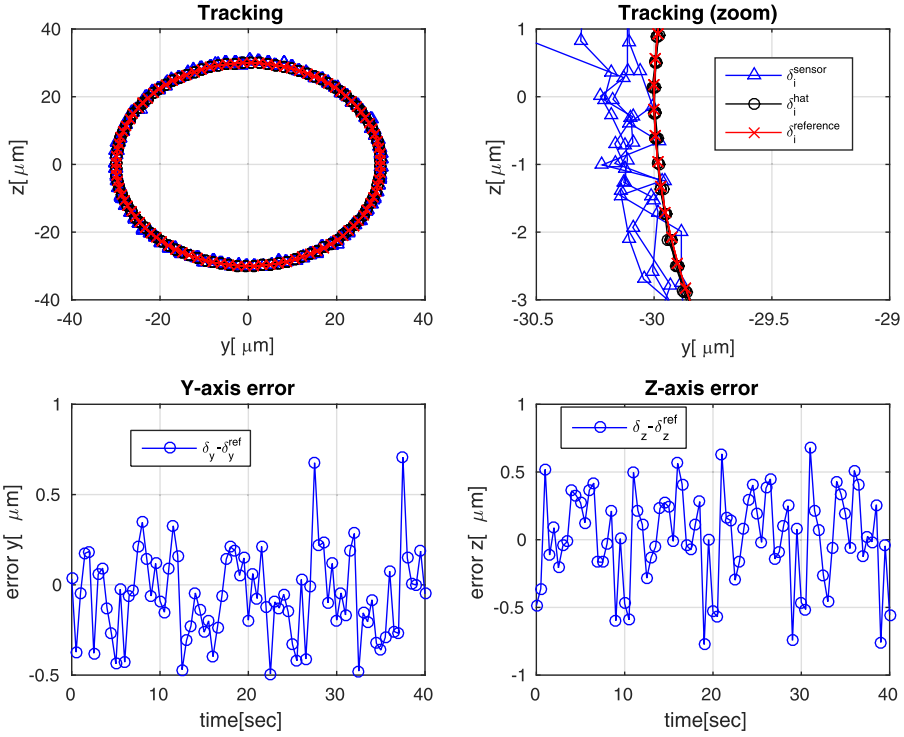

Fig. 14. Closed-loop performance @ 0.1*Hz*.

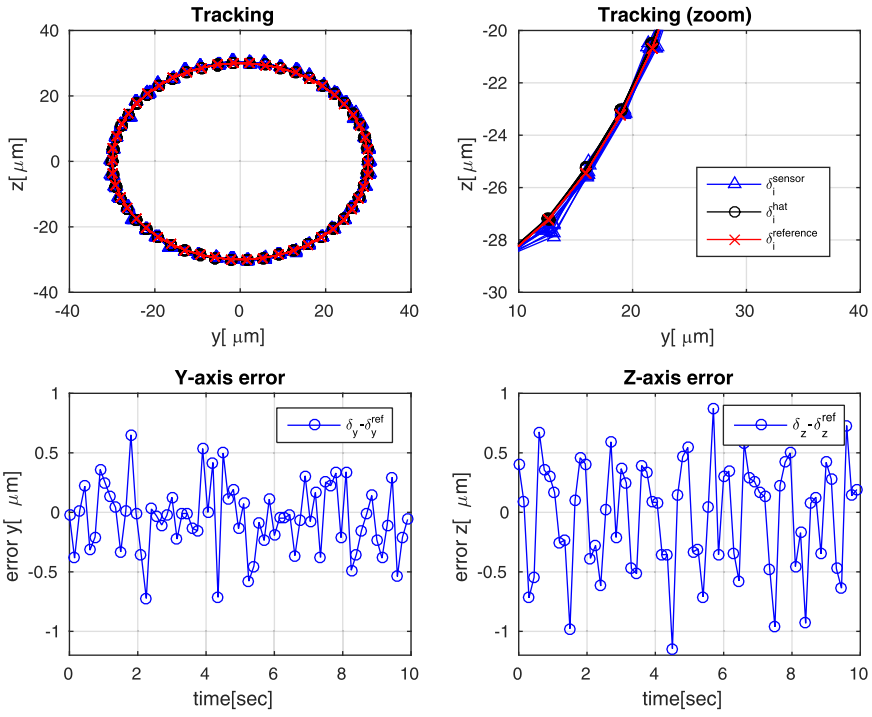

Fig. 15. Closed-loop performance @ 1*Hz*.

2) **Trajectory-tracking case:** In this case the objective is to track a time-varying sinusoidal reference (frequency= $1[Hz]$ and amplitude= 2[μm]).

Remark. In Fig. 9 it is shown that the compensation effect of both controllers ($t > 7.5[sec]$). The PID controller is not able to compensate, while the controller based on the disturbance estimation tracks the reference trajectory satisfactorily. Moreover, at $t = 1.6[sec]$ it is displayed numerically the deviation between both errors witnessing the effectiveness of the proposed strategy.

6. Real-time experimental results

Section 4 has detailed the estimation strategy of the disturbance (dual-axis hysteresis, couplings and creep) as well as the controller design via a constructive design which guarantees GAS considering the bounded actuators. Therefore, in this section it presented the experimental implementation of the proposed strategy to track circular trajectory for both open- and closed-loop. Indeed, the worst-case scenario occurs during simultaneous 2D positioning generating also cross couplings. The

Table 3
Experimental parameters.

Parameter	Value
sampling time T_s	0.2×10^{-3} [sec]
PSD W_{Θ_i}	0.01
R_i	0.04
λ_{1_i}	1.2
λ_{2_i}	1

positioning objective is to track a circular pattern at 0.1[*Hz*] and 1[*Hz*], and whose expressions are defined by the following time-parametrized functions

$$\begin{aligned} &\delta_y(t)^d = 30\sin(2\pi f t) \text{ and } \dot{\delta}_y(t)^d = 60\pi f \cos(2\pi f t) \\ &\delta_z(t)^d = 30\cos(2\pi f t) \text{ and } \dot{\delta}_z(t)^d = -60\pi f \sin(2\pi f t) \end{aligned} \tag{59}$$

Firstly, it is presented the open-loop performance to observe the effect of the disturbance on the system's response while attempting to track circular trajectory. Next, the proposed estimation alongside the controller are included to compensate disturbances resulting from tracking a circular trajectory.

Real-time experiments were carried out using Matlab-Simulink® which is linked to the dSPACE®DAQ[1] via ControlDesk®. Experimental parameters are listed on the Table 3.

6.1. Open-loop experiments

During micro-positioning operations the piezocantilever's performance is significantly deteriorated mainly due to hysteresis and creep. Besides to these adverse effects, multi-DOFs (2DOF in our case) positioning tasks feature internal dynamic couplings, this is shown by the curves matrix in Figs. 10 and 11. In the open-loop case we consider a control input including the desired trajectory without any feedback and/or disturbance estimation, i.e.

$$u = \frac{a}{d_p}\left(\frac{1}{a}\delta^d + \frac{b}{a}\dot{\delta}^d + \ddot{\delta}\right) \tag{60}$$

In Figs. 12 and 13 it is observed that the error between the reference and the position is quite significant reaching up to 30%. It is witnessed the need of incorporating not only a feedback approach but also disturbance-tolerant trajectory-tracking controllers. On the other hand, the good performance of the position estimation and filtering imply that the overall disturbance $\Theta(t)$ is well estimated. Thus at this stage the ES-LKF estimation is validated.

6.2. Closed-loop experiments

The experimental stage, presented next, provides a set of results intended to show the effectiveness of the proposed strategy in presence of parametric and parasitic disturbances. Besides the robustness aspect, it is worthwhile highlighting the following:

- The trajectory-tracking objective is performed using the measured position δ_i and estimated velocity.
- The estimation of the lumped disturbance relies fully on the ES-LKF.

The closed-loop scheme illustrated by Fig. 7 is used to compensate the dynamic dual-axis disturbances arising from simultaneous 2D motion (i.e. a circular trajectory reference) with the estimated generalized disturbance $\hat{\Theta}(t)$. In general, experimental results depicted in Figs. 14 and 15 reveal that motion objective is fulfilled within the actuator voltage limits. Whereas the error reached 30% in open-loop, these figures show that the circular reference, at 0.1[*Hz*] and 1[*Hz*], is successfully tracked having errors below 2% for both axes. It is noteworthy to point out this performance since tracking tasks for second order system requires the knowledge of both states, and therefore the aforementioned results imply not only the effective estimation of $\hat{\Theta}(t)$ but also the good velocity estimation considering that only the position measurement is available.

[1] I/O Acquisition card

7. Concluding remarks

This paper addressed the control of two degrees of freedom (2-DOF) piezoelectric actuator (PEA) devoted to micromanipulation tasks. Although the actuator exhibit interesting bandwidth and positioning resolution, it is typified by strong couplings between its two axes, and strong hysteresis and creep nonlinearities. These couplings and nonlinear phenomena finally compromise the overall performances of the tasks: loss of accuracy, stability compromised.

We have witnessed the effectiveness of the proposed estimation-control strategy not only by fulfilling the objective of a dynamic disturbed trajectory-tracking having only position measurement with an estimated velocity, but also by a successful disturbance ESLKF-based compensation. Moreover, we have shown the flexibility and robustness of the method by presenting two frequency cases and considering a partial knowledge of the a dynamic model (nominal model). In this paper, we proposed a new strategy to control 2-DOF PEAs for microrobotics tasks. This strategy is based on two steps : firstly, an estimation of the hysteresis, creep and couplings is implemented with a ES-LKF. The unknown dynamic of this disturbance is simply modeled by a random walk process (Wiener process). Secondly, this estimation is used in a feedback scheme to compensate for this disturbance. Extensive experiments were carried out and demonstrate the efficiency of the proposed approach of modeling and control for low frequency trajectory tracking despite the simplicity of the feedback used. More elaborated control architecture should be developed to deal with high-speed tracking.

Acknowledgments

This work was partially supported by the Labex-ACTION (ANR-11-LABX-0001-01). This work was also partially supported by the French Investissements dAvenir program, project ISITE-BFC (contract ANR-15-IDEX-03).

References

[1] RV Iyer XT, Krishnaprasad P. Approximate inversion of the preisach hysteresis operator with application to control of smart actuators. IEEE Transactions on Automatic Control 2005;50(6).
[2] Croft GSD, Devasia S. Creep, hysteresis and vibration compensation for piezoactuators: atomic force microscopy application. ASME Journal of Dynamic Systems, Measurement and Control 1999;123(50).
[3] Dubra JMA, Paterson C. Preisach classical and nonlinear modeling of hysteresis in piezoceramic deformable mirrors. Optics Express 2005;13(22).
[4] Rakotondrabe M. Multivariable classical prandtl-ishlinskii hysteresis modeling and compensation and sensorless control of a nonlinear 2-dof piezoactuator. Springer Nonlinear Dynamics (NODY) 2017;89(1):481–99. doi:10.1007/s11071-017-3466-5.
[5] Mokaberi B, Requicha AAG. Compensation of scanner creep and hysteresis for afm nanomanipulation. IEEE Transactions on Automation Science and Engineering 2008;5(2).
[6] Rakotondrabe M. Classical prandtl-ishlinskii modeling and inverse multiplicative structure to compensate hysteresis in piezoactuators. American Control Conference 2012.
[7] Janaideh MA, Krejci P. Inverse rate-dependent prandtl-ishlinskii model for feedforward compensation of hysteresis in a piezomicropositioning actuator. IEEE/ASME Trans Mechatron 2013;18(5).
[8] Rakotondrabe M. Bouc-wen modeling and inverse multiplicative structure to compensate hysteresis nonlinearity in piezoelectric actuators. IEEE Transactions on Automation Science and Engineering 2011;8(2).
[9] Didace Habineza MR, Gorrec YL. Bouc-wen modeling and feedforward control of multivariable hysteresis in piezoelectric systems: application to a 3-dof piezotube scanner. IEEE Transactions on Control Systems Technology 2015. doi:10.1109/TCST.2014.2386779.
[10] Lin F-J, Shieh H-J, Huang P-K, Teng L-T. Adaptive control with hysteresis estimation and compensation using rfnn for piezo-actuator. Ultrasonics, Ferroelectrics, and Frequency Control, IEEE Transactions on 2006;53(9):1649–61. doi:10.1109/TUFFC.2006.1678193.

[11] Lin F-J, Shieh H-J, Huang P-K. Adaptive wavelet neural network control with hysteresis estimation for piezo-positioning mechanism. Neural Networks, IEEE Transactions on 2006;17(2):432–44. doi:10.1109/TNN.2005.863473.
[12] Li Y, Xu Q. Adaptive sliding mode control with perturbation estimation and pid sliding surface for motion tracking of a piezo-driven micromanipulator. IEEE Transactions on Control System Technology, 2010;18(4):798–810. doi:10.1109/TCST.2009.2028878.
[13] Chen X, Hisayama T. Adaptive sliding-mode position control for piezo-actuated stage. Ind Elect IEEE Trans 2008;55(11):3927–34. doi:10.1109/TIE.2008.926768.
[14] Sebastian MVSA, Cleveland JP. Robust control approach to atomic force microscopy. Conf Decis Control 2003.
[15] Micky Rakotondrabe YH, Lutz P. Plurilinear modeling and discrete mu-synthesis control of a hysteretic and creeped unimorph piezoelectric cantilever. IEEE Int Conf Autom Robo Control Vision 2006.
[16] Sofiane Khadraoui MR, Lutz P. Combining h-inf approach and interval tools to design a low order and robust controller for systems with parametric uncertainties: application to piezoelectric actuators. Int J Control 2012;85(3).
[17] Boudaoud M, Haddab Y, Le Gorrec Y. Modeling and optimal force control of a nonlinear electrostatic microgripper. Mechatron IEEE/ASME Trans 2013;18(3):1130–9. doi:10.1109/TMECH.2012.2197216.
[18] Rakotondrabe M, Lutz P. Force estimation in a piezoelectric cantilever using the inverse-dynamics-based uio technique. In: Robotics and Automation, 2009. ICRA '09. IEEE International Conference on; 2009. p. 2205–10. doi:10.1109/ROBOT.2009.5152178.
[19] Piat E, Abadie J, Oster S. Nanoforce estimation with kalman filtering applied to a force sensor based on diamagnetic levitation. In: Intelligent Robots and Systems (IROS), 2011 IEEE/RSJ International Conference on; 2011. p. 39–44. doi:10.1109/IROS.2011.6094457.
[20] Fleming AJ. A review of nanometer resolution position sensors: operation and performance. Sens Actuators, A 2013;190:106–26. doi:10.1016/j.sna.2012.10.016.
[21] Sepulchre R, Janković M, Kokotović P. Constructive Nonlinear Control. Communications and control engineering; W.H. Freeman, 1997. Ed. Springer